A Numerical Study of an Intense Quasi-stationary Convection Band over the Korean Peninsula

Jianhua SUN and Tae-Young LEE

Laboratory for Atmospheric Modeling Research/Department of Atmospheric Sciences, Yonsei University, Seoul, Korea

(Manuscript received 3 July 2001, in revised form 28 June 2002)

Abstract

An intense long-lived, quasi-stationary convection band that occurred on 5–6 August 1998 over the middle of the Korean peninsula, was studied using both observation and a numerical model. The convection band persisted for more than 10 hours, and produced heavy rain along the band with a maximum of 619 mm in 15 hours at a coastal station (Kanghwa). Radar observation indicates that the convection band is 20–30 km wide, and about 300 km long at its mature stage. It consists of several long-lived precipitation cells along the band. Some of the precipitation cells develop on the west coast, and move northeastward along the band. The convection band occurred over the middle of the Korean peninsula, where a converging airflow pattern is found between the mid latitude cyclone to the north, and the western Pacific subtropical high to the south.

The simulated convection band forms and evolves in a consistent manner with the observation, although it shows notable differences from the observation in the onset time, lifetime and rainfall intensity. Formation of the simulated band proceeds in the following manner. First, new convection cells continuously form on the west coast and move northeastward forming a line of long-lived convection cells. Second, a line of low-level convergence forms somewhat rapidly in the upwind side of the convection initiation point, and then convective cells develop and move along this line. Some cells develop into deep convection and last several hours. These processes result in a long convection band. The favorable large-scale condition (especially the converging airflow), and its interaction with convection, seem to be the important elements for the development of the present convection band. Surface latent heat flux is found to play a crucial role in establishing a convectively unstable environment for the onset of convection. It is also found that orographic effect is not an essential factor for the formation of the present convection band.

1. Introduction

A significant portion (normally 53%) of the annual precipitation on the Korean peninsula is produced by heavy rainfall during summer (KMA 2001). Many of the heavy rains occur during the summer monsoon period. The humid weather with frequent heavy rain in Korea is called the Jangma (like Baiu in Japan and Meiyu in China), and it normally starts in mid June and lasts for about a month. Heavy rainfalls also occur often in August.

Heavy rain can be produced by disturbances of several types in Korea. For example, some heavy rainfalls are generated by disturbances that originate in China, and propagate eastward along the Jangma front (Park et al. 1986; Lee et al. 1998). Sometimes, heavy rain is caused by a convection band, which develops locally over the Korean peninsula. Typhoons are also important contributors of heavy rain during summer.

Heavy rainfalls, associated with convection

Corresponding author: Tae-Young Lee, Department of Atmospheric Sciences, Yonsei University, Seodaemoon-Ku, Seoul 120-749, Korea.
E-mail: lty@atmos.yonsei.ac.kr

bands, have been observed over the Korean peninsula and have caused heavy loss of lives and property. One noticeable heavy rainfall occurred on 5–6 August 1998 (Fig. 1). In this incident, an intense and quasi stationary convection band persisted for more than 10 hours and produced a large amount of rain over an elongated area with a record breaking rainfall amount (619 mm in 15 hours) at a coastal station (Kanghwa).

Convection band is an important mode of organized convection and frequently occurs in many regions of the world including East Asia. Several convection bands in subtropical environments, have been observed over the Kyushu Islands, Japan (e.g., Yoshizumi 1975; Ninomiya and Yamazaki 1979; Ogura et al. 1985; Yoshizaki et al. 2000), and around Taiwan (Li et al. 1997; Teng et al. 2000; Yu et al. 1999). Unlike the fast moving squall lines, these convection bands are slow moving or quasi stationary in general. Akiyama (1979) and Ninomiya and Yamazaki (1979) suggested that the large scale environment and features of mesoscale convective systems of the Baiu frontal zone, were different from those of severe local storms and squall lines over the United States, tropical squall lines, and polar frontal cyclones. Yoshizumi (1975) reported an instability line (convection band), which occurred in the southeast quadrant of the large-scale vortex in the vicinity of Kyushu, whose synoptic circulation was very similar to that for the present case.

Orographic forcing is suggested to play an important role in the formation of the convection bands around the Kyushu Islands, and Taiwan. In addition, Ninomiya et al. (1988) suggested the possible role of symmetric instability in the formation of a precipitation band over Kyushu in the presence of a strong vertical wind shear.

Another important feature of heavy rain on the Korean peninsula is that it is closely associated with the low-level jet (LLJ), which is also found for Baiu and Meiyu (Matsumoto 1973; Ninomiya and Murakami 1987; Tao and Chen 1987; Chen and Yu 1988). Kim et al. (1983) found that heavy rainfalls during Jangma were found horizontally in between the upper-level jet (ULJ) to the north, and the LLJ to the south. Hwang and Lee (1993) found that 88 percent of the heavy rainfall events during the period of 1980–1989 were accompanied by LLJ. Recently, Lee et al. (1998) suggested that a strong convergence ahead of the LLJ region played a key role for production of the heavy rain associated with an eastward propagating disturbance.

Although the convection band, and heavy rain of 5–6 August 1998 over the Korean peninsula have attracted serious attentions of researchers and operational meteorologists in Korea, its structure and formation mechanism are still poorly understood. To improve the prediction of this type of convective system, it is essential to understand the formation, and maintenance of the convection band.

This study focuses on understanding the formation and evolution mechanism of the convection band of the 5–6th August 1998 over the Korean peninsula. Observational analysis of the case is given in section 2. The descriptions of the atmospheric model, the experimental design and the initializations are provided in section 3. Results of the control experiment and the formation mechanism are discussed in section 4. In order to extract the role of surface forcings, results of several sensitivity experiments are analyzed in section 5. Finally, conclusions are given in section 6.

2. Overview of synoptic conditions

2.1 Precipitation system

From the 3rd to the 6th August 1998, heavy rain of 100–600 mm day^{-1} occurred over the middle of the Korean peninsula. This study has concentrated on the most intense convective activity, during the period of 00 UTC (09 LST) 5–00 UTC (09 LST) 6 August. UTC time lags behind the local standard time (LST) for Korea by 9 hours. The heavy rain during this 24-h period was produced by a well-organized convection band (see Figs. 1 and 4). During the period, a record-setting heavy rain of 619 mm occurred at a coastal station, Kanghwa (its location is marked by "+" in Fig. 1), and rainfall of 351.5 mm was recorded at Dongdoochon (marked by "*" in Fig. 1). A significant feature of hourly precipitation at these two stations (Fig. 2) was that most rainfall was concentrated within the 12-h period of 18 LST 5–06 LST 6 August. The maximum hourly rainfall of 112 mm was observed between 01 and 02 LST 6 August at Kanghwa (Fig. 2b). The analysis

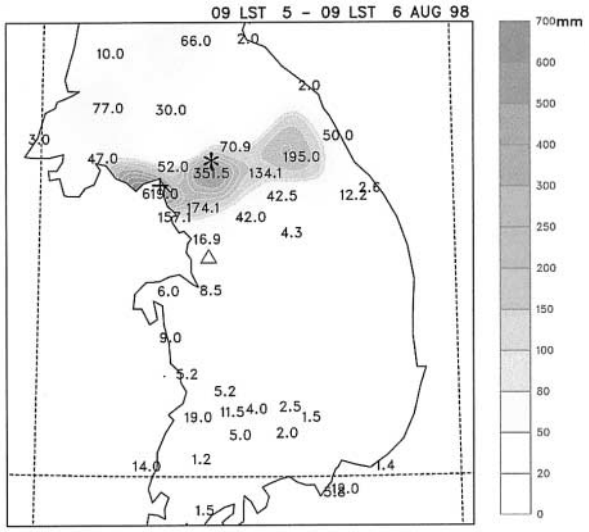

Fig. 1. Observed 24-h precipitation from 0900 LST 5 to 0900 LST 6 August 1998. Contours are for 20, 50, 80, 100, 150, 200, 250, 300, 400, 500, 600 mm. Area of rainfall exceeding 20 mm is shaded. Kanghwa, Dongdoochon and Osan are indicated by "+", "∗" and "Δ", respectively.

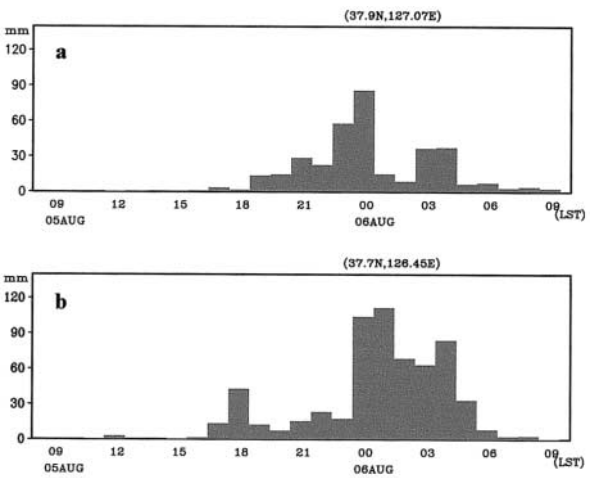

Fig. 2. The observed hourly precipitation at (a) Dongdoochon and (b) Kanghwa during 0900 LST 5–0900 LST 6 August 1998.

for other stations, at which heavy rain occurred during this event, also indicated that the most intense rain occurred from midnight to early morning.

Enhanced GMS satellite infrared imagery shows a synoptic-scale cyclonic system over northeastern China, and its associated clouds extended to the East Sea (the Sea of Japan) (not shown). A small convective system appears on the west coast, in the middle part of the Korean peninsula, at 15 LST 5 August (Fig. 3). Afterwards, a band of cloud develops over the middle of the peninsula, and persists until 7–8 LST 6 August.

According to the radar images, several heavy precipitation cells occur after 15 LST 5 August along a loosely defined wide band of rain area, being extended from the Yellow Sea to the middle of the Korean peninsula (not shown). Such pattern is maintained until about 1900 LST. The convection band that interests us begins to develop after 1900 LST, when a few small convection cells develop at the location of line formation (on the west coast, indicated by an arrow in Fig. 4 for 1900 LST 5 August). A short and narrow line of weak echo appears on the coastal area at 1930 LST (indicated by an arrow). This line is extended both toward the sea, and inland. At 2030 LST, its length over the land has become more than 40 km. At this hour, the existing precipitation cells to the south are also being extended inland.

The line continues to develop in its extent and strength. It has moved southeastward by about 15 km, to the line location at 2100 LST. Then the seaward development of the echo line proceeds somewhat rapidly after 2100 LST, and a long convection band has formed at 2130 LST. Echo intensity along the line is mostly weak during this formative stage (1900∼2130 LST). The echo shows a continuous line structure in general, although several cells, with relative stronger intensities, are visible along the line. At 2200 LST, the convection band over the land is less distinct than that over the sea, due to the existing precipitation cells to its immediate south, which are aligned in parallel to the band. The band over the land and the existing cells become integrated, and a line of strong convection develops in the inland area, near the coast at 2230 LST. After this hour, precipitation cells with strong rainfall intensity keep developing along the band, especially over the land area near the coast.

The radar images also show that the convection cells move along the band (Fig. 4). The

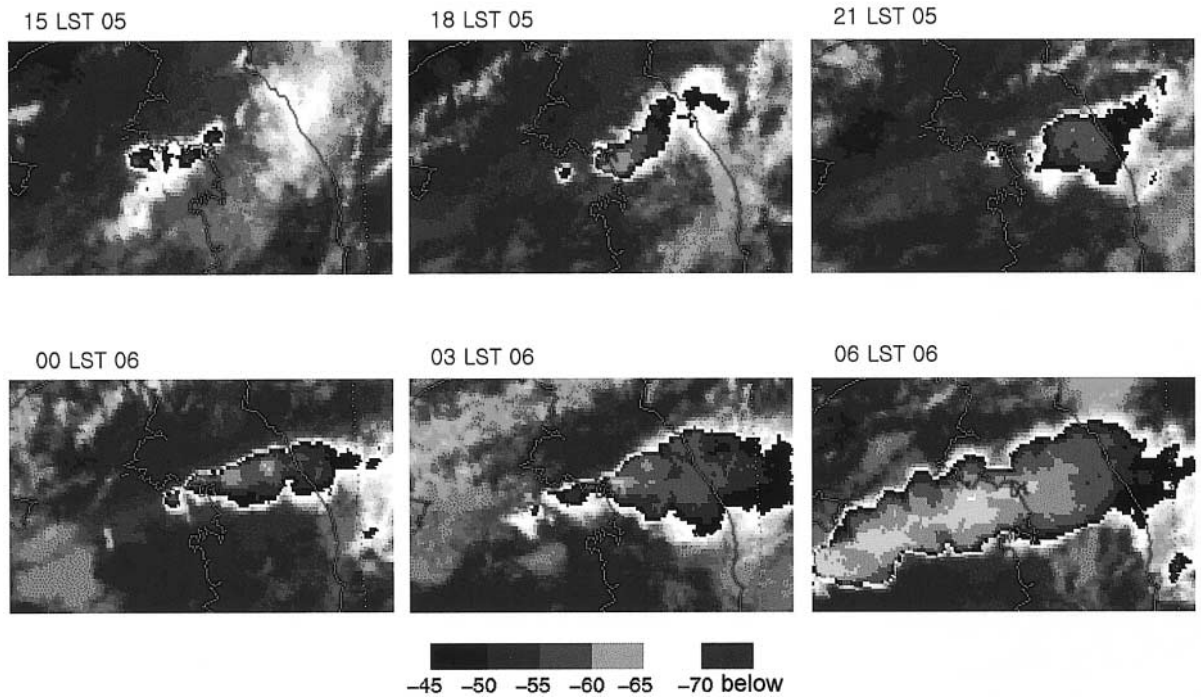

Fig. 3. Enhanced GMS infrared satellite imagery for the period 1500 LST 5–0600 LST 6 August 1998. Numbers on the scale bar represent brightness temperature (°C).

rainfall intensity tends to be stronger as the convection cell propagates on the west coast. Figure 4 also indicates that the band itself has moved eastward as noticed by the change in the band location over the sea after 2200 LST 5 August. A new band development occurs over the sea after 0000 LST 6 August. As a result, a band of convection cells appears again over the sea at 0100 LST, and develops into a well-defined band at 0200 LST (not shown). This band is maintained at nearly the same location, until about 0700 LST 6 August, and then moves southward and slowly disintegrates (not shown). The radar images indicate that the convection band is 20–30 km wide, and about 300 km long at the mature stage.

2.2 Weather pattern

At 00 UTC 5 August, a synoptic-scale cyclone at 850 hPa was located over northern China, with its major axis in the northwest-southeast direction (Fig. 5a). Its center moved eastward and became located to the north of the Korean peninsula at 12 UTC (21 LST) 5 August (Fig. 5b). A minor ridge occupied the Korean peninsula and the East Sea on 4 August (not shown) and shifted eastward to the East Sea and Honshu on 5 August 1998 (Figs. 5a and b). The Western Pacific Subtropical High (WPSH) extended to the Kyushu Islands on 5 August 1998, and a belt of relatively strong southwesterly or low-level jet (LLJ) developed along the northwestern edge of the WPSH. Thus, warm and moist air was transported to the Korean peninsula by the strong low-level southwesterly.

The present convection band developed in the area between the synoptic scale cyclone to the north, and the WPSH to the south. The 850-hPa height pattern at 12 UTC (21 LST) 5 August indicates that there is a converging airflow (southwesterly flow to the south and westerly flow to the north of the band) over the middle of the Korean peninsula (Fig. 5b).

At 500 hPa, the 5880-gpm height contour, the periphery of WPSH, extends towards the middle of the peninsula, during 3rd–4th August (not shown). The 5880-gpm height contour has moved northwestward, and the mid-latitude trough has moved southeastward to the middle Korean peninsula on 5th August. This move results in an intensification of the geopotential

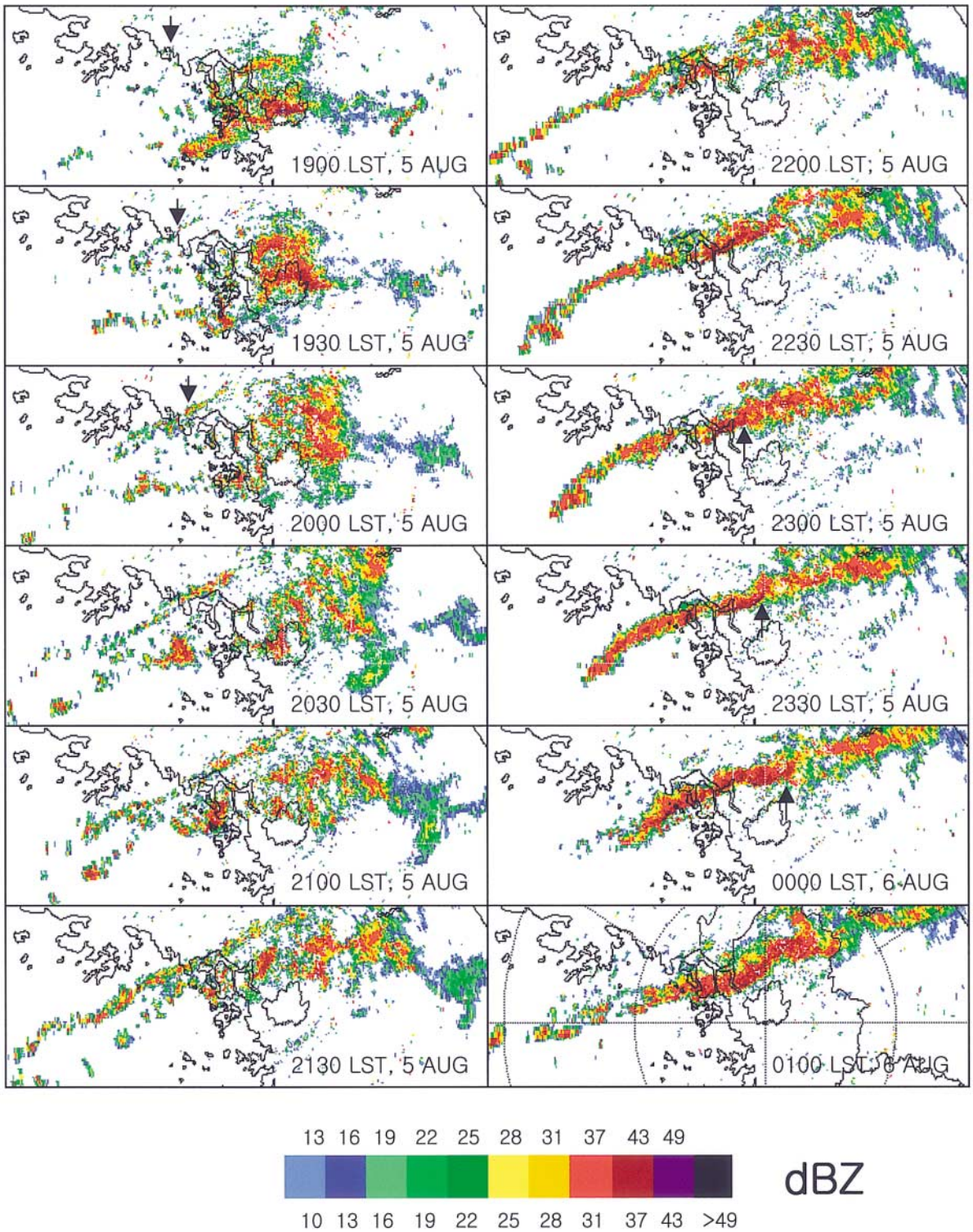

Fig. 4. Radar images showing the distribution of reflectivity for the period 1900 LST 5 August–0100 LST 6 August 1998. Arrows in the images for 1900–2000 LST are pointing at the initial band formation, while the arrows for 2300 LST 5–0000 LST 6 August are pointing at the same precipitation cell to show its movement. The circles in the image for 0100 LST 6 August are the radius ranges of 100 and 200 km.

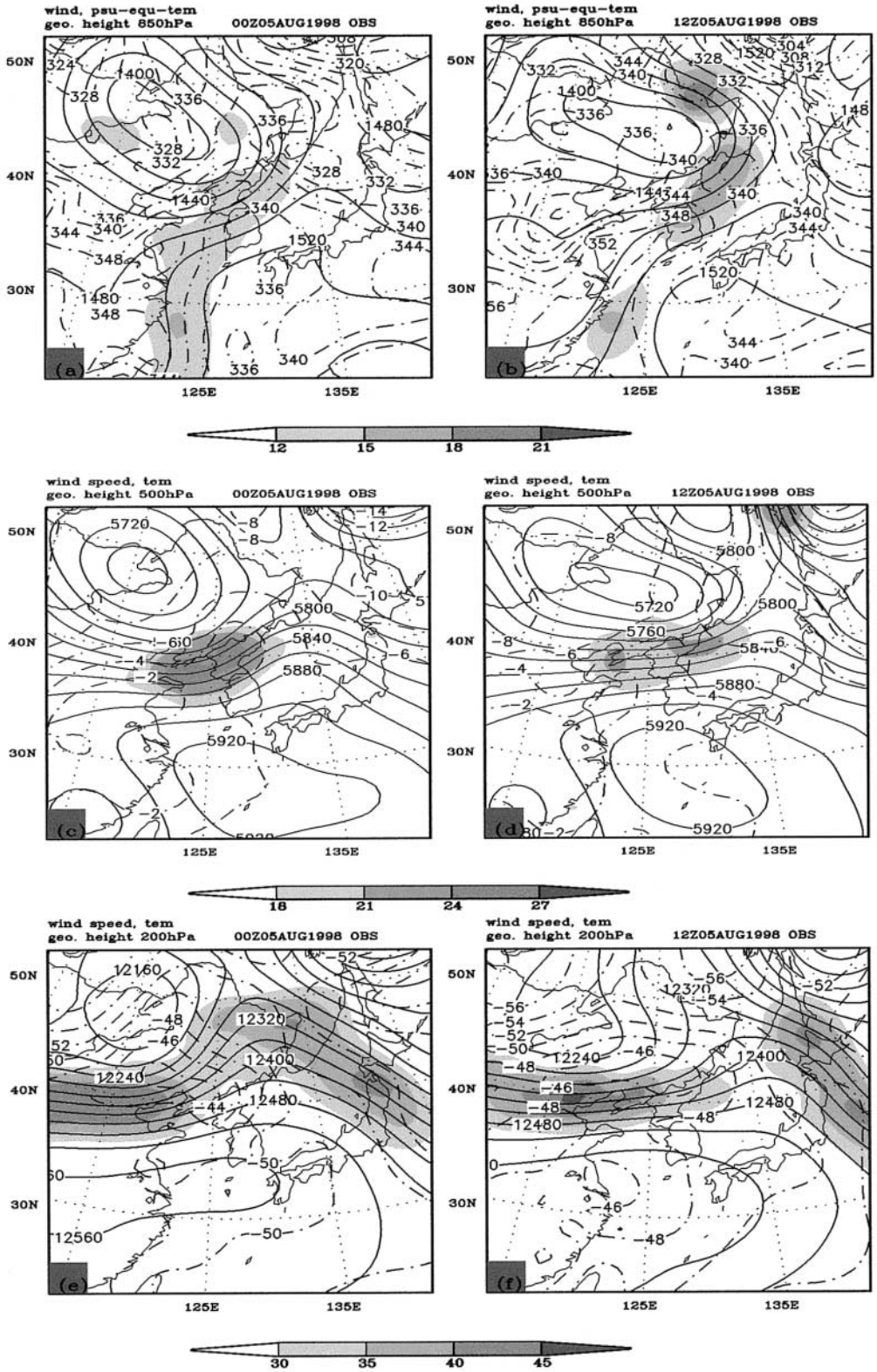

Fig. 5. Upper panels (a) and (b) represent the observed geopotential height (solid line, gpm), pseudo-equivalent potential temperature (dashed line, K), and wind speed (shaded, m s^{-1}) fields at 850 hPa for 0000 and 1200 UTC 5 August 1998, respectively. Middle and bottom panels show the geopotential height (solid line, gpm), temperature (dashed line, °C) and wind speed (shaded, m s^{-1}) for 500 and 200 hPa, respectively.

height gradient, producing a strong westerly flow exceeding 18 m s^{-1} over the northern and central parts of the Korean peninsula (Figs. 5c and d). A midlevel jet, dry and cold advection behind the cyclone in the middle troposphere, may have contributed to the destabilization of the low- and mid-troposphere. Over the central part of the Korean peninsula, the southwesterly wind has shifted to a westerly direction at 12 UTC on 5th August.

In the upper troposphere, the upper-level westerly jet with maximum speeds higher than 30 m s^{-1} is found between 38–42°N over the northern part of the Korean peninsula at 12 UTC on 5th Aug (Fig. 5f). A weak to moderate shear is found in the upper troposphere. It has been indicated by Maddox (1983), and Laing and Fritsch (1997) that upper-tropospheric jet streaks, with moderate shear and baroclinicity, are common to MCC environments. In the present case, the convection band is located to the south of the exit region of the upper-level jet streak (Fig. 5f). For a typical jet streak, downward motion may be expected in the southern side of the exit region (Hoskins et al. 1978; Shapiro and Kennedy 1981). However, in the present case, the height and vorticity fields (not shown) at 200 hPa do not show such a typical pattern. Instead, quasi-geostrophic analysis indicates the presence of weak, to moderate upward motion in the upper layer between 200 and 500 hPa over the middle, and northern parts of the peninsula at 12 UTC (not shown). This large-scale upward motion, due to quasi-geostrophic forcings, may provide a favorable condition for the development of convection band. Model results also show the presence of upward motion over the middle of the peninsula before the convection band develops.

The corresponding synoptic situation at surface indicates that a low-pressure center is located over northeastern China, and a cold front extends toward the Korean peninsula at 00 UTC on 5th August (not shown). However, analyses of surface temperature, dew-point temperature and wind, do not show any indication of a front over the middle of the peninsula during the period of initiation and development of the convection band. It is possible that fine mesoscale features may have been missed in this analysis, because of lower spatial and temporal resolution of surface synoptic observations.

The synoptic scale flow pattern over the middle of the peninsula did not change significantly during the evolution of the convection band, although the cyclone over northern China moved eastward. The high-pressure system, to the south of the convection band, did not show any move. Westerly, to the north of the band, was also maintained during the evolution period. The synoptic features, such as the nearly constant WPSH, and the quasi-steady converging airflow in the northwestern edge of the WPSH, may be important environmental conditions for the persistency, and quasi-stationary behavior of the present convection band.

It is well known that LLJ transports warm and moist air northward, creates a convectively unstable layer (Chen 1983; Ninomiya and Akiyama 1974), and induces a secondary circulation with an ascent at the northern tip of the LLJ (Chen 1982), which may be essential for the development of heavy precipitation. In the present case, the convective system forms, and develops at the northern edge of the relatively strong southwesterly or LLJ over the Korean peninsula. Thus, the southwesterly seems to contribute to the development of a convection band, by transporting moisture to the convection area. Yoshizumi (1975) suggested that the low-level jet played an important role in the organization of cumulus convection into a band. Strong convergence ahead of LLJ was found to be an important element for the development of heavy rain in the case of an eastward propagating storm (Lee et al. 1998). But the present case does not seem to show such direct dynamic forcing for heavy rain development.

To further investigate the atmospheric conditions for the development of convection, the rawinsonde sounding over Osan, at the time of band formation (2100 LST 5 August), was analyzed (Fig. 6). Osan is located at about 70–80 km south of the band (marked by "Δ" in Fig. 1). A thin inversion layer is found at 800 hPa between the moist lower layer, and the dry upper layer. Very dry air dominates the upper levels from 500 hPa to 300 hPa. The sounding during the evolution of an intense convection band also exhibits the same characteristics (not shown). The dry air at the mid troposphere becomes wet after the heavy rainfall has finished (not shown). The mid-tropospheric dry air in-

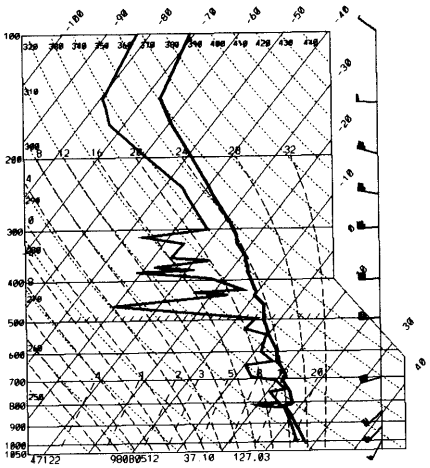

Fig. 6. Observed upper-air sounding at Osan (127.03°E, 37.10°N) for 1200 UTC (2100 LST) 5 August 1998. The full barb and the flag represent 5 m s^{-1} and 25 m s^{-1}, respectively. Temperature and dew points are in °C.

tensifies the convective instability ($-\partial\theta_{se}/\partial p$), where θ_{se} is the pseudo-equivalent potential temperature. Wind blows in the direction of SW-WSW below 700 hPa, but westerly prevails at levels above 500 hPa. The wind shear from the surface to 700 hPa is about 10–15 ms^{-1}, while the wind shear is relatively weak in the mid troposphere.

3. The mesoscale model and model initialization

The present convective system has been studied further using a mesoscale model. The model and initialization are described here.

3.1 The mesoscale model

The PSU-NCAR three-dimensional, non-hydrostatic mesoscale model (MM5 version3) is used for the present study. A two-way interactive, nested grid system is used to include three domains (Fig. 7). They consist of a 45-km grid domain (D01, 100 × 100 grid points), a 15-km grid domain (D02, 121 × 121 grid points) and a 5-km grid domain (D03, 121 × 121 grid points). The model top is located at 100 hPa. The 24 vertical sigma levels are 1, 0.99, 0.98, 0.96, 0.93, 0.89, 0.85, 0.8, 0.75, 0.7, 0.65, 0.6, 0.55, 0.5, 0.45, 0.4, 0.35, 0.3, 0.25, 0.2, 0.15, 0.1, 0.05, and 0.0. The presentation will focus on the results for the 5-km grid domain.

The microphysics for explicit moisture processes is treated using the mixed-phase microphysics scheme of Reisner et al. (1998), in which five prognostic equations are solved for mixing ratios of water vapor, cloud water, rainwater, cloud ice, and snow. The cumulus parameterization scheme of Grell (Grell et al. 1991) is employed for subgrid-scale convection in coarse grids. Blackadar's high-resolution scheme (Blackadar 1979; Zhang and Anthes

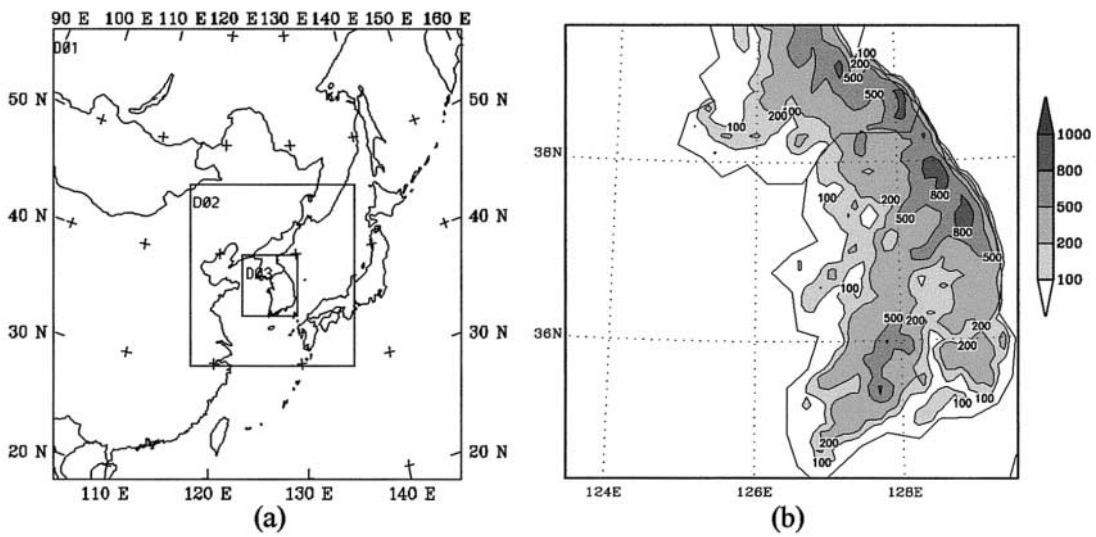

Fig. 7. (a) The computational domains and (b) the topography in domain3 (D03). The contours are for 100, 200, 500, 800 and 1000 m.

1982) is adopted to calculate the turbulent fluxes in the PBL. Physics options for the 15- and 5-km grid simulations, are the same as the coarse-grid simulation except that subgrid scale convection is not considered. The five-layer soil model of Dudhia (1996) is employed to predict soil temperature. Soil moisture is prescribed using the global land-use data in MM5.

3.2 Model initialization

6-hourly global analyses (00 UTC 5–00 UTC 6 August), with 2.5° resolution from the National Centers for Environmental Prediction (NCEP), are interpolated horizontally to model grid points. Then the standard radiosonde and surface observations are analyzed using a successive correction scheme on the base of first guess. No balancing between mass and wind fields is performed. Finally, the analyses are interpolated to the model σ levels. The numerical integration starts at 00 UTC (09 LST) 5 August 1998. The time-dependent, lateral boundary conditions are obtained by interpolating the 6-h observational analyses linearly in time. No other special observations are available for the present case. Thus, it may be a serious challenge for the model to simulate the initiation, and evolution of the convection band, using only conventional observation data.

4. Simulated convection band

The simulated convection band is initiated at nearly the right location, and the simulated precipitation pattern agrees fairly well with the observation. On the basis of successful simulation, the simulated results are utilized to document the detailed structure of the convection band, and the possible mechanisms responsible for the formation and development of a convection band. Subsection 4.1 presents the comparison of simulated results, with the available observations. The initiation and evolution of a simulated convection band and propagation of embedded convective cells are discussed in subsection 4.2. The three-dimensional structures of the intense convection band, and the individual cells during its mature stage, are presented in subsection 4.3.

4.1 Comparison of the simulation with observation

Comparison between the simulation, and the observation is made using the hourly rainfall amount in Fig. 8 for the period from 18 LST 5 to 05 LST 6 August. Since hourly rainfall data for North Korea are not available, the observations are represented by numbers (hourly rainfall amount in mm) at station locations for South Korea only. The simulated hourly precipitation pattern matches fairly well with the observed rain belt, especially for the period 21 LST 5–02 LST 6 August, during which the band forms and develops. Therefore, we will concentrate more on this period in the following discussions.

The comparison shown in Fig. 8 indicates that the simulation has not reproduced the significant rainfall before 2100 LST 5 August, which was produced by the preexisting precipitation system. One possible reason for this failure might be the short spin-up time (about 6 hours) to simulate the preexisting system, which developed after 1500 LST. It is also found that the simulated system begins to move southward at around 0200 LST 6 August, whereas the observed system is quasi-stationary until 0700 LST 6 August. This may be an important limitation of the present simulation. The earlier southward move of the simulated band may be due to the incomplete simulation of the synoptic-scale cyclone to the north of the peninsula.

The maximum amount of simulated rainfall occurs at a grid (37.7°N, 126.3°E) near Kanghwa, as that in the observation. The time series of simulated hourly rainfall amount at this location is shown in Fig. 9. Simulated temporal distribution matches very closely with the observation, although the simulated rainfall is significantly smaller and ends earlier than the observation. The reason for the significant underprediction of rainfall amount is not yet well understood, although the initial data, grid size and model physics may be among the possible causes. The shorter duration of the simulated rainfall at this location can be attributed to the earlier southward propagation of the simulated convection band.

The results have been examined further to understand the simulated atmospheric structure during the initiation and development of the convection band. Figure 10 shows the simulated horizontal flow and the vertical velocity at 925 hPa for the period of 18 LST 5–04 LST 6 August. The simulated flow for 18 LST

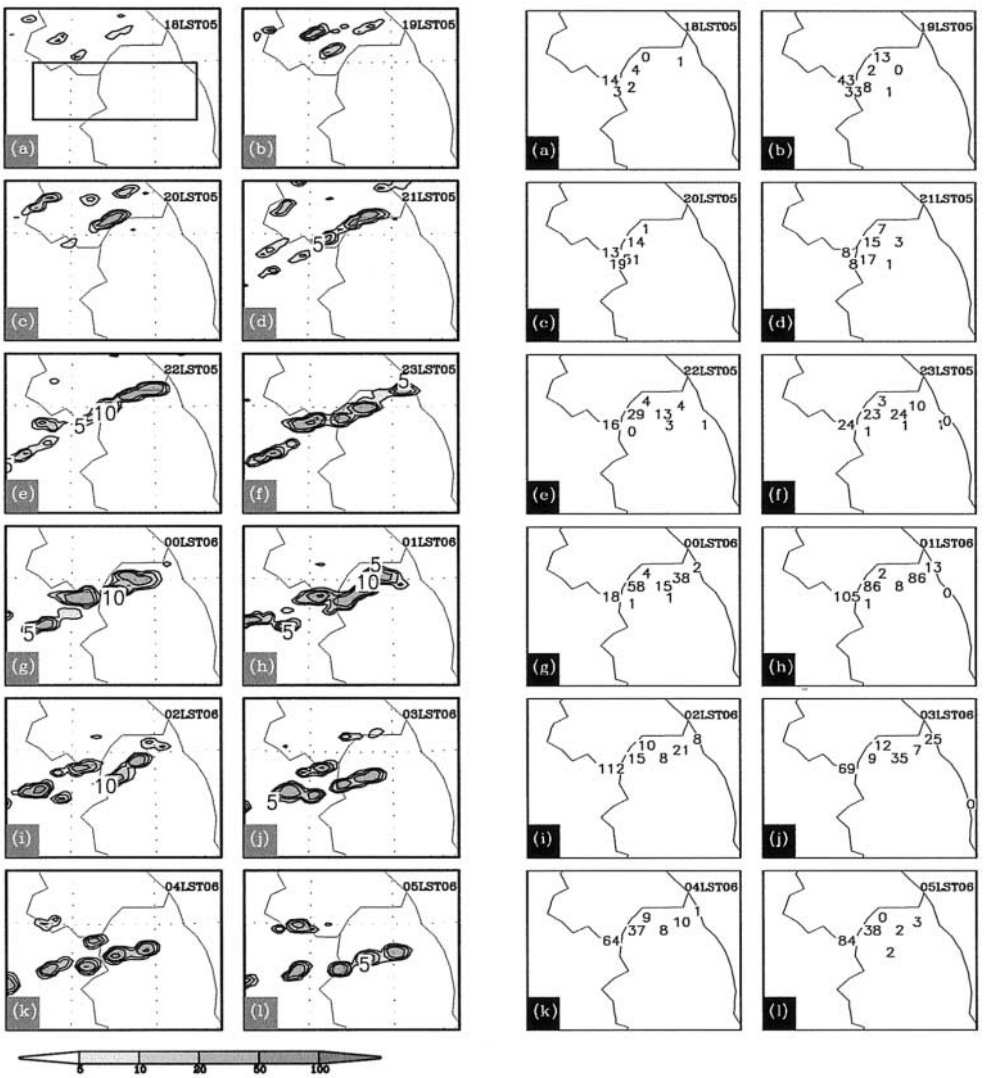

Fig. 8. The simulated (left panels), and the observed (right panels), hourly precipitation from 1800 LST 5 (0900 UTC 5) to 0500 LST 6 (2000 UTC 5) August 1998. The contour values are 5, 10, 20, 50, 100 mm, and the areas above 5 mm are shaded. The box in the top panel on the left is the analysis area for the results shown in Figs. 18 and 19.

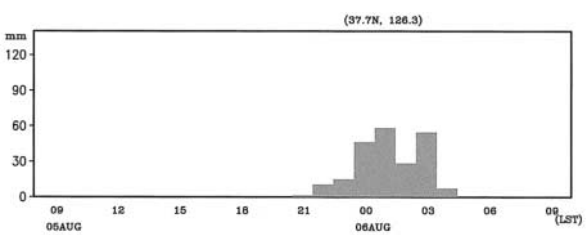

Fig. 9. The simulated hourly precipitation at 126.3°E, 37.7°N during 0900 LST 5–0900 LST 6 August 1998.

5, shows that a southwesterly dominates most of the Korean peninsula (Fig. 10a). The figure shows the gradual change of the wind direction over the northern part, and a nearly constant southwesterly over the southern half of the fine grid domain. This differential change of wind between the north and south allows the development of an elongated zone of strong convergence between these two flow regimes (over the middle of the Korean peninsula). However, the convergence zone is limited to the lower tropo-

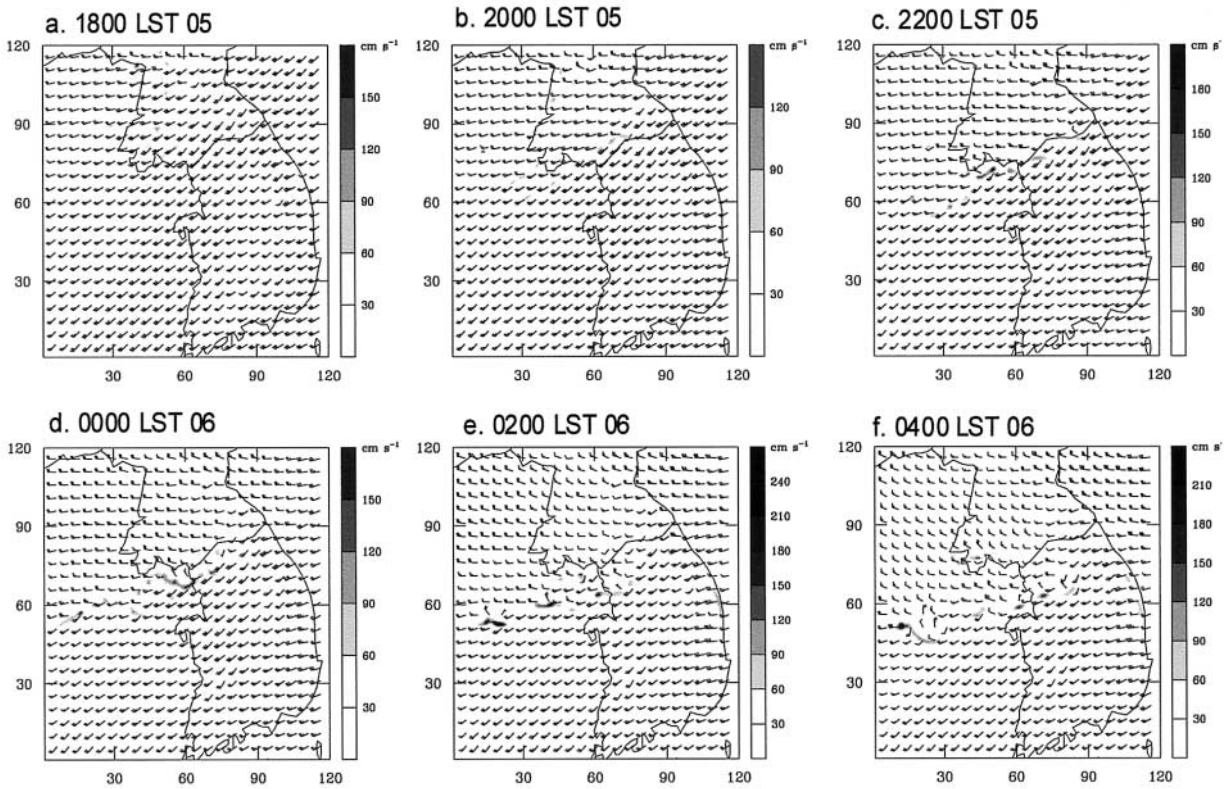

Fig. 10. Simulated wind fields (the full bar represents 5 m s^{-1}) and vertical velocity at 925 hPa (shaded) for (a) 1800 LST 5, (b) 2000 LST 5, (c) 2200 LST 5, (d) 0000 LST 6, (e) 0200 LST 6, and (f) 0400 LST 6 August 1998. Shading indicates the area with vertical velocity greater than 30 cm s^{-1}. The grid numbers are labeled along the axes of abscissa and ordinate.

sphere, since the airflow over the area becomes more uniform at higher levels (e.g., 700 hPa).

The differential change of wind seems to be partially associated with the different behavior of pressure systems around the convection band. The change over the northern side (southern part of the synoptic cyclone), seems partially due to the eastward move of the synoptic cyclone center to the north of the Korean peninsula. On the other hand, the flow over the southern half is mainly associated with the WPSH, which does not show any significant change during this event. However, the role of convection seems to be essential for the formation of a strong mesoscale convergence zone, which has been noted in the sensitivity experiment in section 5. It enhances the convergence, and also affects the wind fields around it.

The westerly area gradually expands southward with time, and the convergence over the sea becomes stronger. The convergence line has not moved much until 00 LST 6 August (Fig. 10d). After 0200 LST, it travels southward as the westerly over the northern side changes into a northwesterly (Figs. 10e and f). The northwesterly causes the line to propagate southward. The comparison of the simulated and observed pressure pattern (not shown) has revealed that the simulated cyclone propagates eastward faster than that of the observation. As a result, the northwesterly region behind the simulated cyclone arrives at the northern peninsula earlier than the observation, causing the wind fields over the northern side of the convection band to change into northwesterly earlier. As previously mentioned, this may be a reason why the southward move of the simulated band occurs earlier than that of the observation. It is not clear what causes the model to produce faster eastward movement of the synoptic scale cyclone to the north of the convection band.

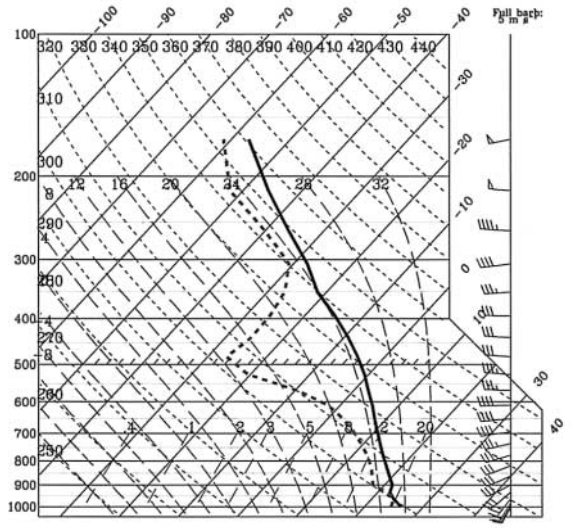

Fig. 11. Simulated profiles of temperature (solid line, °C) and dew point temperature (dashed, °C) at Osan (37.10°N, 127.03°E) for 2100 LST (1200 UTC) 5 August 1998.

The simulated sounding at Osan, for 12 UTC (21 LST) 5 August (Fig. 11) is quite similar to the observation (Fig. 6). It shows the moist lower, and upper troposphere, and dry middle troposphere. The wind direction veers from the southwesterly at lower troposphere to the westerly in the middle and upper troposphere. Although the simulated sounding is very similar to that of observation, some significant distinctions between the simulation and the observation are found. The simulated wind speed below 900 hPa is somewhat stronger than that of the observation. The saturated layer does not extend to the observed height (about 800 hPa), and the height of the simulated dry layer is a little lower than that of the observation.

The comparison indicates that the simulated convection band shows consistencies with the observation in its location and extent, and in the manner of band development. On the other hand, the simulation disagrees with the observation in that the simulated line has a shorter lifetime, and produces significantly weaker rainfall intensities, than the observation. The quality of simulation will be further discussed in the next section after comparing the detailed evolution of the convection band, with observation.

4.2 Formation of convection band and the propagation of embedded convection cells

The simulated fields are analyzed further to explain the formation and the development of the convection band. The stream lines at 925 hPa, and the radar reflectivity at 850 hPa, are shown in Fig. 12 for the period 1630 LST–2030 LST 5 August at an interval of 30 minutes, to illustrate the process of convection band formation. Reflectivity is calculated using the simulated mixing ratios of rain and snow. Convective cells develop somewhat in a random pattern in the early hours, but show a tendency to develop in lines at later hours (Figs. 12e–i). Some weak convective cells, which do not give significant rainfall and disappear quickly, also occur over North Korea in the simulation, whereas those cells were not found on the satellite and radar images. This is one of the flaws of the present simulation study. The southernmost convection band, located over the middle of the Korean peninsula, becomes dominant and develops into a well-defined convection band at about 2030 LST, being oriented in the southwest-northeast direction (Fig. 12i).

Three convection cells along the dominant convection band are indicated by "1", "2", "3" to show their sequential movement and development. Cell 1 forms on the west coast of the middle of the peninsula at 1630 LST, and a new cell (Cell 2) also forms at the same location at 1730 LST, as Cell 1 moves northeastward. Simulated echo band also appears over the sea at 1800 LST. Then the seaward development of band proceeds somewhat rapidly. Convective cells develop along the band over the sea at 2000 LST forming a long band of convection cells. This result indicates that the simulated convection band forms about 1.5 hours earlier than the observed band shown in Fig. 4. However, the evolution of band proceeds very similarly to the observation in the following senses: 1) its formation is initiated by the convection cells over the coastal area; 2) the band develops both landward and seaward; 3) the seaward development proceeds somewhat rapidly; and, 4) the band itself moves eastward (movement of simulated band can be found in Fig. 14).

The convection cells move northeastward with a speed of 50 km h^{-1} during the formation period. The lifetime of Cell 1 is about 5–6 hours. These results are somewhat consistent

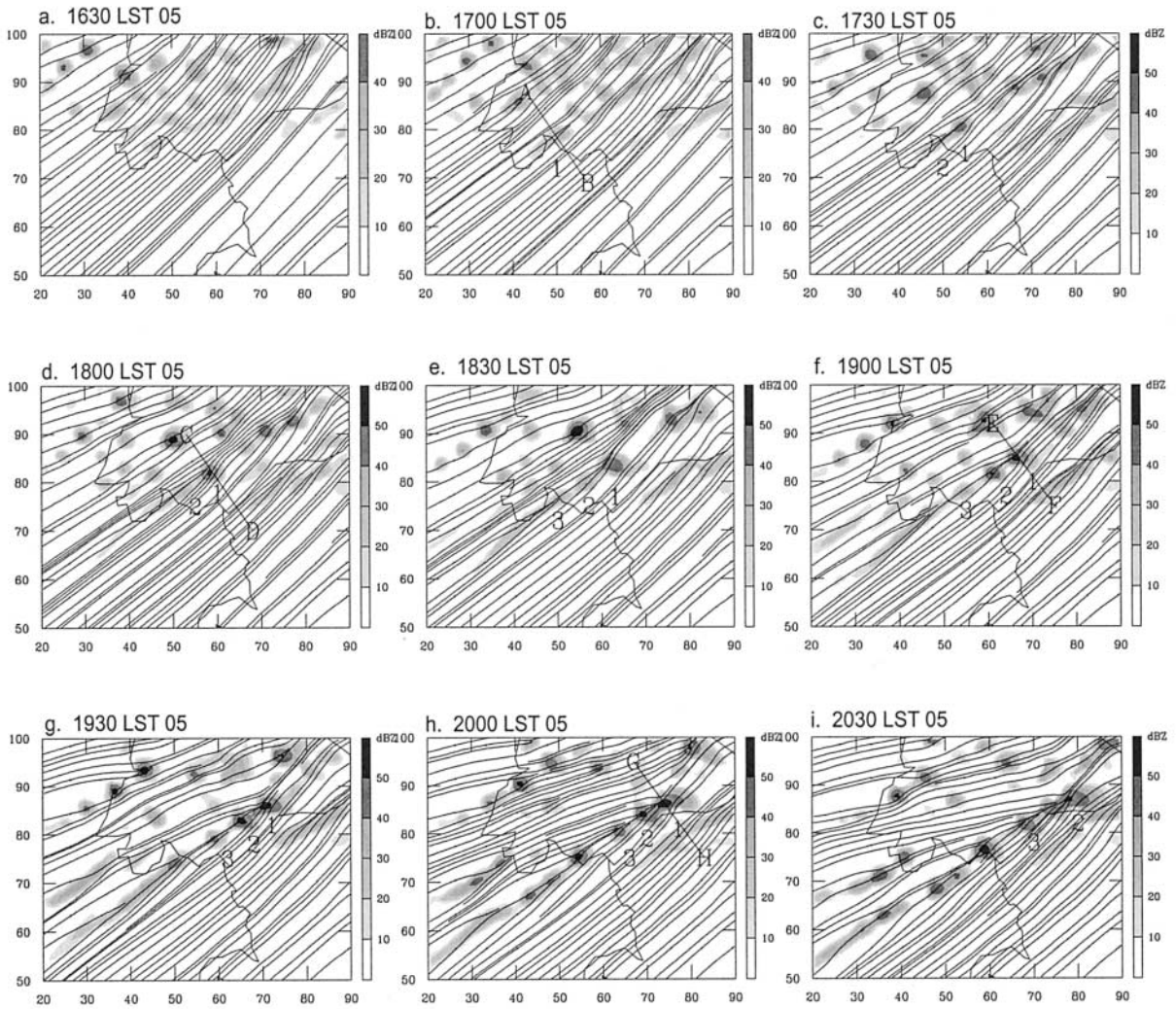

Fig. 12. Simulated streamlines at 925 hPa and radar reflectivity at 850 hPa (shaded, dBZ) for the period 1630 LST (0730 UTC)–2030 LST (1130 UTC) 5 August 1998 at an interval of 30 minutes. Three convective cells are indicated by "1", "2", and "3" to trace them, and the four lines marked by "AB", "CD", "EF" and "GH" represent the location of cross sections shown in Fig. 13. The grid numbers are labeled along the axes of abscissa and ordinate.

with the radar observation (Fig. 4), and the observed hourly precipitation, which also starts on the west coast in the middle of the peninsula and then gradually extends northeastward (Fig. 8). However, the simulated band tends to show a cell-type echo structure more than the observation, although it also shows line-shaped rain area as in the observation. Another discrepancy is that the existing precipitation cells to the south of the band, have not been simulated well, as previously mentioned.

Although the model results show several notable discrepancies from the observation, the simulated band appears to form and evolve in a consistent manner with the observation. And both the observation and simulation indicate that the width of the convection band is 20–30 km. The horizontal size of simulated convection cells ranges from 10 to 100 km. It can be pointed out that the grid size of 5 km may not be adequate for proper simulation of narrow band, and small cells. To find out if the results are seriously affected by the use of finer grid size, an experiment with 1.67 km grid

has also been carried out. The results indicate that the major features of simulated convection band found from the 5-km grid simulation, are not much changed by the use of finer grid, although the 5-km grid model has a limit in simulating the fine structure of the band. It also has been found that the simulated rainfall amount does not increase significantly with the decrease of grid size. Thus, the results of 5-km grid simulation are further analyzed to investigate the mechanism of convection band development.

Synoptic scale winds seem to be the primary factor for the movement of the convection cells. The wind profile near the convection band shows the vertical variation of wind direction: SW below 800 hPa, SWW at 700 hPa and W above 600 hPa (see Fig. 11). The direction and speed of initial cell movement shown in Fig. 12 are close to those of the winds below 800 hPa.

Figure 13 shows the cross sections following Cell 1: "AB", "CD", "EF" and "GH" (as indicated in Fig. 12). It can be found that the convection cell is initiated at low-level (Figs. 13a and b). At an hour after the formation, the convection has developed up to middle troposphere (below 8 km) with the strongest vertical velocity of 4 ms^{-1} (Figs. 13c and d). The convection does not intensify much further after 1800 LST, but its strength is well maintained for the next 2 hours (Fig. 13c–h).

The present analysis indicates that the development of the convection band proceeds in two steps. First, new convection cells continuously form on the west coast and move northeastward forming a line of convection cells. Second, a line of low-level convergence forms somewhat rapidly over the sea in the upwind side of the convection initiation point, and then convective cells develop and move along this line. Convection cells develop into a deeper convection as they move and last several hours. These processes result in a long convection band.

In order to explain the convection band formation, the following questions should be addressed: 1) why do cells continuously form on the west coast, and move along the band; 2) how do the cells develop into a deeper convection, and maintain their strength for several hours; 3) why does this convection band develop in that particular location; and, 4) how does the low-level convergence line form over the sea.

The more interesting question may be what brings the convection band to this particular location. The important factors for the location of the band development appear to be the availability of large-scale convergence, and the strong low-level moisture transport from the south. Availability of both factors is found over the middle of the Korean peninsula, just to the north of the southwesterly belt associated with the WPSH. A zone of large-scale convergence develops over the middle of the Korean peninsula when the winds to the north of the band change into westerly as previously explained for Fig. 10. The convection cells from the west coast move along this zone and enhance the flow convergence contributing to the development of a sharp convergence line, which then allows the development and maintenance of the propagating convection cells. It seems that this interaction between convection, and large-scale convergence, is very important for the development of the present convection band. The low-level moisture transport from the south is also very important for the development of convection band as can be found later in Fig. 16.

At present, it is not clear why the convection cells develop continuously on the west coast, and why the convergence line forms over the sea. These points remain to be studied further in the future.

4.3 The structure of the simulated convection band

As shown in the previous subsection, a well-defined convection band develops over the middle of the Korean peninsula at about 2030 LST 5 August (Fig. 12i). The evolution of model-produced radar reflectivity at 850 hPa for the period of 2200 LST 5–0200 LST 6 August indicates that the convection band moves southeastward slowly. At the same time, a new development occurs over the sea, consequently forming a new convection band at about the same location (Fig. 14). This is consistent to some extent with the radar observations (see the description related to Fig. 4). But the two-line structure, and the early southward move of the band over the land at 0200 LST, are not found in the observation. Therefore, the well-

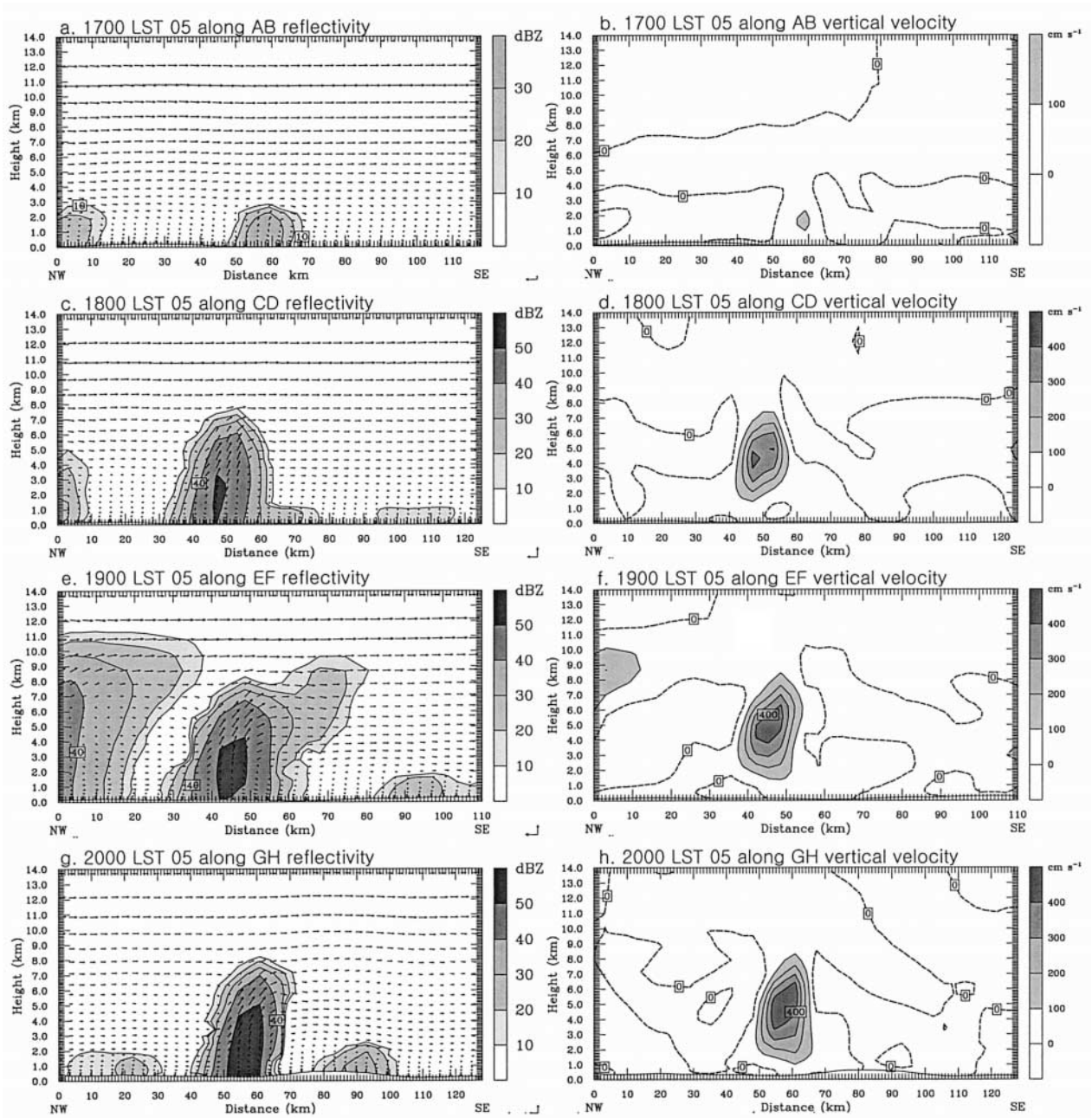

Fig. 13. Vertical cross sections of reflectivity (left panel, dBZ) and vertical velocity (right panel, cm s^{-1}) along the lines "AB", "CD", "EF" and "GH" shown in Fig. 12. Wind vector is composed of the horizontal wind along the cross section and vertical velocity.

organized convection band at 2200 LST 5 August is analyzed to find out the dynamic, and thermodynamic, structure of the convective system at its mature stage.

Figure 15 shows the vertical structure of the simulated convection band along the line AB in Fig. 14a. The convection band consists of several embedded convective cells with the spatial scale of 50–100 km and its maximum reflectivity exceeds 50 dBZ (Fig. 15a). The convection cells extend up to 14-km height. The strength of the southwesterly along the band gradually increases with height, and a moderate vertical shear is found.

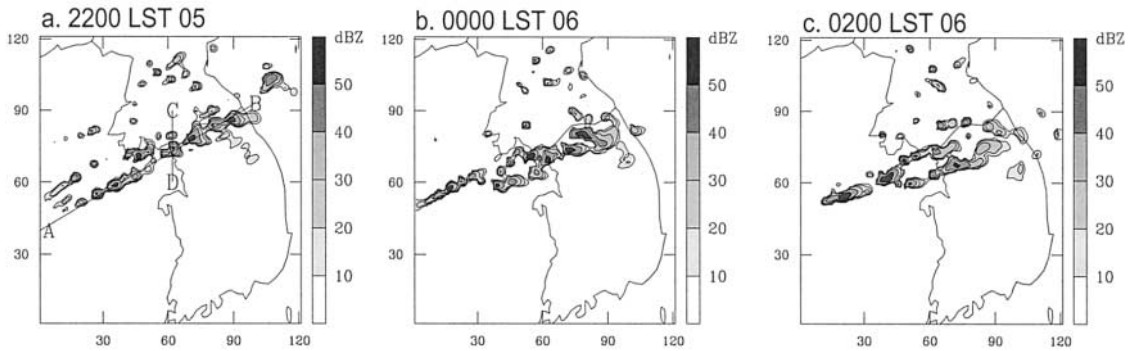

Fig. 14. Simulated radar reflectivities (dBZ) at 850 hPa for (a) 2200 LST 5 (1300 UTC 5), (b) 0000 LST 6 and (c) 0200 LST 6 August 1998.

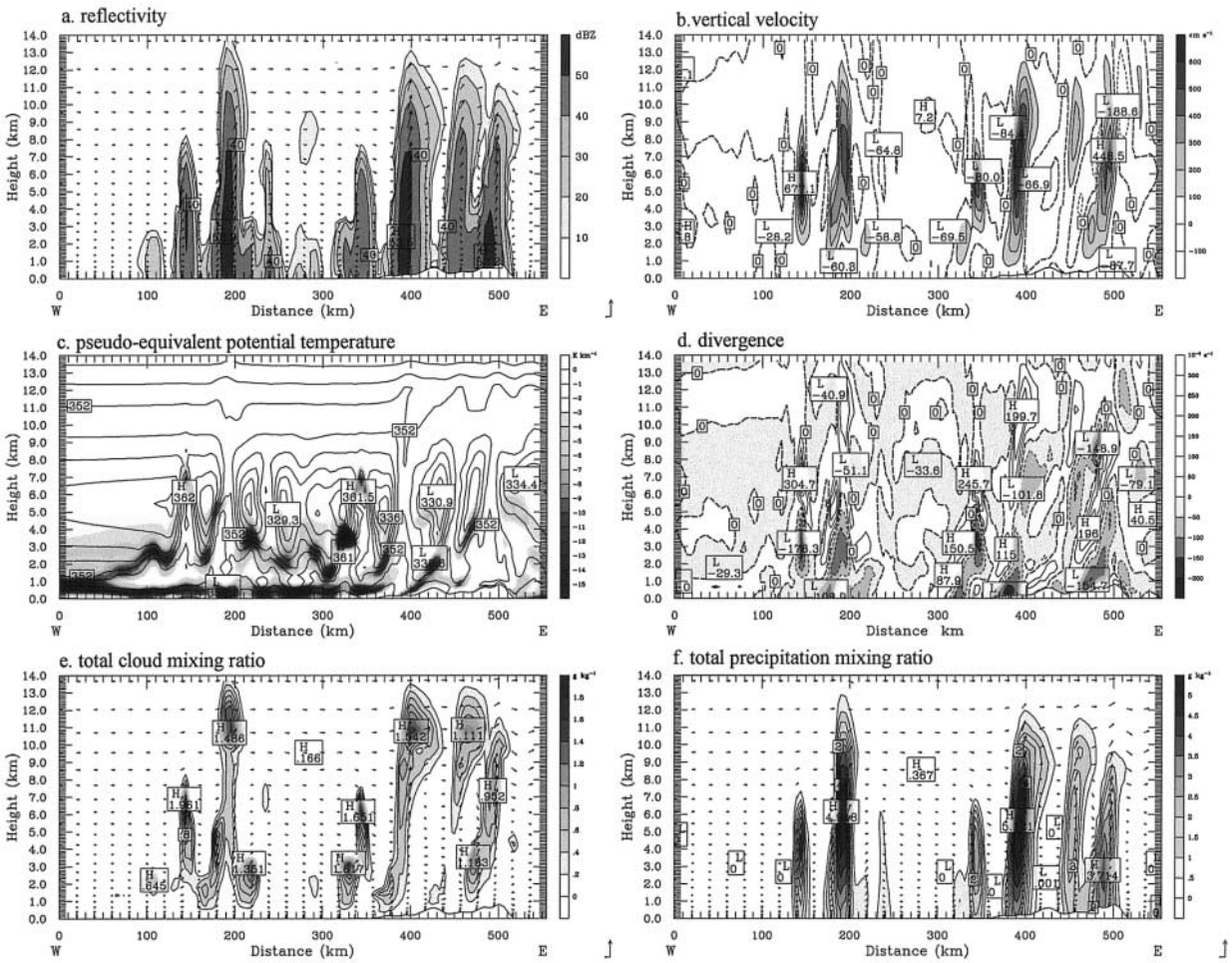

Fig. 15. Vertical cross sections along the line AB in Fig. 14a for 2200 LST 5 (1300 UTC 5) August 1998: (a) reflectivity (dBZ), (b) vertical velocity (cm s^{-1}), (c) pseudo-equivalent potential temperature (K) and convective instability (K km^{-1}), (d) divergence (10^{-5} s^{-1}), (e) total cloud mixing ratio (g kg^{-1}), and (f) total precipitation mixing ratio (g kg^{-1}). Wind vector is composed of horizontal wind along the vertical cross section and vertical velocity.

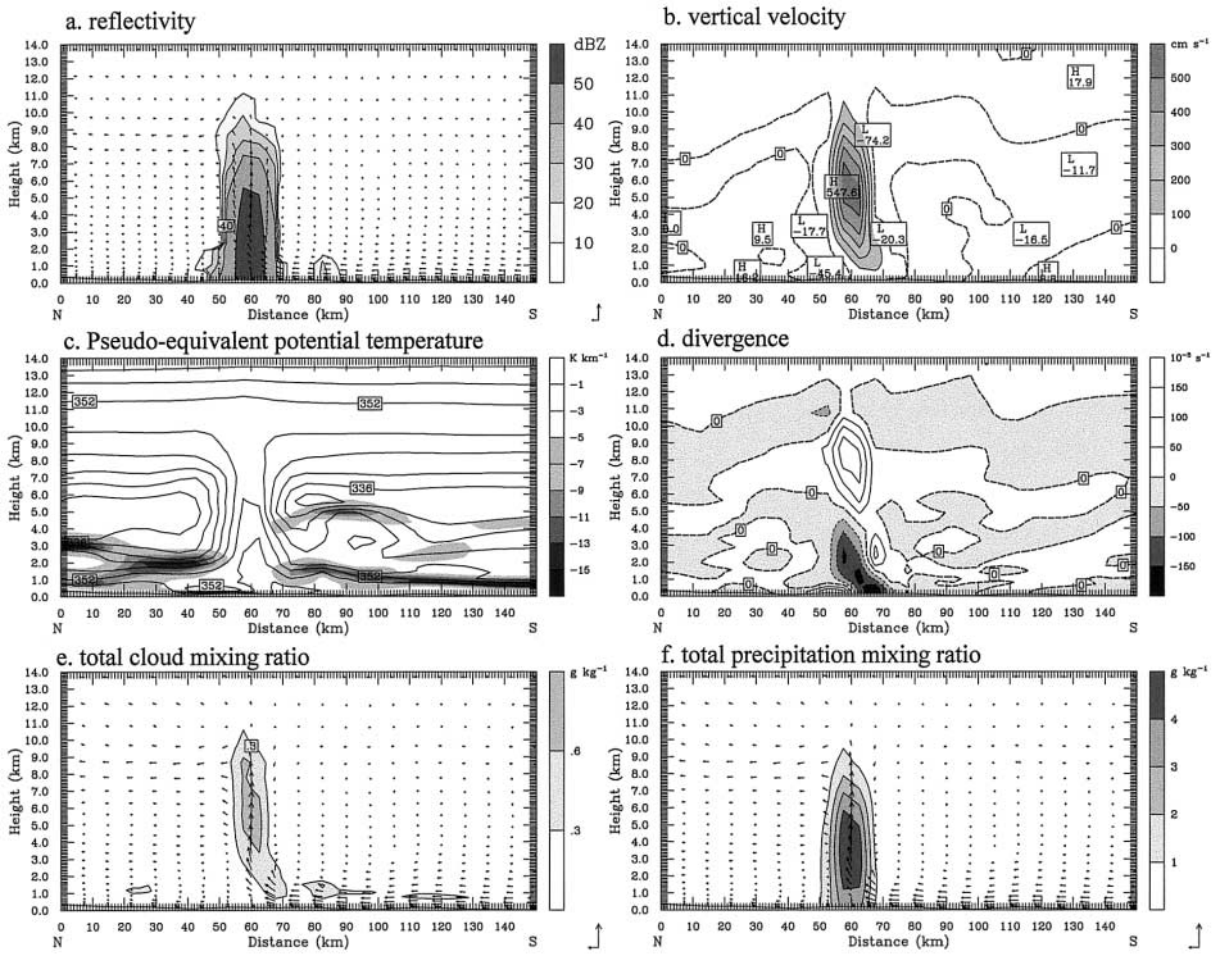

Fig. 16. Same as Fig. 15, except for the line CD in Fig. 14a.

The north-south vertical cross sections of an intense convective cell (the line CD in Fig. 14a) are shown in Fig. 16. The distinct character of the simulated convective cell can be seen in the pronounced vertical structure. The strongest updrafts are located at mid troposphere (5–8 km) (Figs. 15b and 16b), and the subsidence less than 2 ms^{-1}, exists between the convective cells. The pseudo-equivalent potential temperature and convective instability ($\partial\theta_{se}/\partial z$) along the lines AB (Fig. 15c), and CD (Fig. 16c), show the presence of unstable stratification below 5 km, especially in the layer below 1.5 km. Hence, as an intense convection develops, the vertical mixing can consume some of the convectively available energy. Convection results in a nearly neutral stratification in the lower and middle troposphere. It seems that the low-level unstable stratification is an important condition of the development of convective cells.

In the intense convection cells, strong convergence can be found below 5 km, with the strongest convergence exceeding 15×10^{-5} s^{-1} (Figs. 15d and 16d). The convergence zone in the lower troposphere tilts northward. There are two cores of cloud mixing ratio in the intense convection cells (Fig. 15e), one being located in the lower or middle troposphere, and the other one composed of ice in the upper troposphere (10–13 km).

It can be seen that the low-level southwesterly flow supplies warm and moist air to the convective system (Fig. 16e). Most of this inflow becomes the updraft. And a significant outflow is found at the top of the convection cell, and extends far to the north. We define the southern, and the northern sides of the convection, as "ahead" and "behind," respectively.

Ahead of the convection, weak downward motion with speeds of less than 1.0 ms^{-1} exists at the middle and upper levels. Behind the convection, the cooler downdraft with a maximum speed of 0.45 m s^{-1} occurs at the lowest level in the area between 50–60 km, where significant precipitation occurs (Fig. 16). This downdraft enhances the convergence at the location between 60–70 km, and consequently the updraft. However, it does not seem to be the most crucial factor for the development of strong updrafts when we consider its strength. Other factors will be discussed later in section 5. Because of the lack of intensive mesoscale observational data, the structure of the simulated convection band could not be verified. The updrafts tilt northward below about 2 km, and stand upright above 2 km. These features allow the continued development of convection, and significant precipitation.

The present convection band shows both similarities and dissimilarities to other convection bands. It shows some partial similarities in its structure, such as the low-level inflow ahead of the band, and the cooler downdraft behind the band, which allow continued convection development. However, unlike the squall lines, the updraft is partially tilted (only below 2 km) and the convection cells propagate along the band. The favorable large scale flow pattern, and its interaction with convection, may be important for the maintenance of the present convection band, while the continuous inflow of warm and moist air enhanced by the propagation of the squall line may be important for the maintenance of the convective systems in squall lines. Another important difference from the convection bands observed around the Kyushu Islands, and Taiwan, is that orography does not play an important role in the formation of the present convection band (to be discussed in the next section).

5. The impacts of surface forcing on convective system

Sensible (H_S), and latent (H_L) heat fluxes from the sea surface, are known to play an important role in the development of hurricanes (Rotunno and Emanuel 1987) and squall lines (Tao and Soong 1991). Sensitivity experiments have been carried out to examine the influences of various surface forcings on the development of the present convection band (Table 1). In order to isolate the impacts of H_L and H_S, either H_L or H_S is set to 0 in the first three experiments. Both H_L and H_S are neglected in the NOFL experiment. In NOEV, both H_L and H_S are calculated as in CONT, but the surface moisture flux is assumed to be 0 in the calculation of vertical moisture diffusion term for the first grid level above the ground. This is to find out the relative importance of the direct and indirect effects of surface latent heat flux on the development of convection band. The remaining experiments are performed to illustrate the influences of the terrain and land use characteristics on the convection band.

5.1 Sensitivity of simulated precipitation

The precipitation patterns from the control (CONT) and sensitivity experiments are shown in Fig. 17. The amount of rainfall is small when H_L is set to 0 (NOLF) as in Fig. 17b. As mentioned in the previous section, the convective cells on the west coast propagate northeastward resulting in the development of a low-

Table 1. Summary of numerical sensitivity experiments

Experiment Name	Feature
NOLF	No latent heat flux
NOLF2	No latent heat flux after 9-h simulation
NOSF	No sensible heat flux
NOFL	No latent and sensible heat fluxes
NOEV	Same as CONT, except that surface moisture flux is assumed to be 0 only in vertical moisture diffusion term
TERR	Flat terrain over the Korean peninsula
LDUSE	The Korean peninsula is replaced by sea

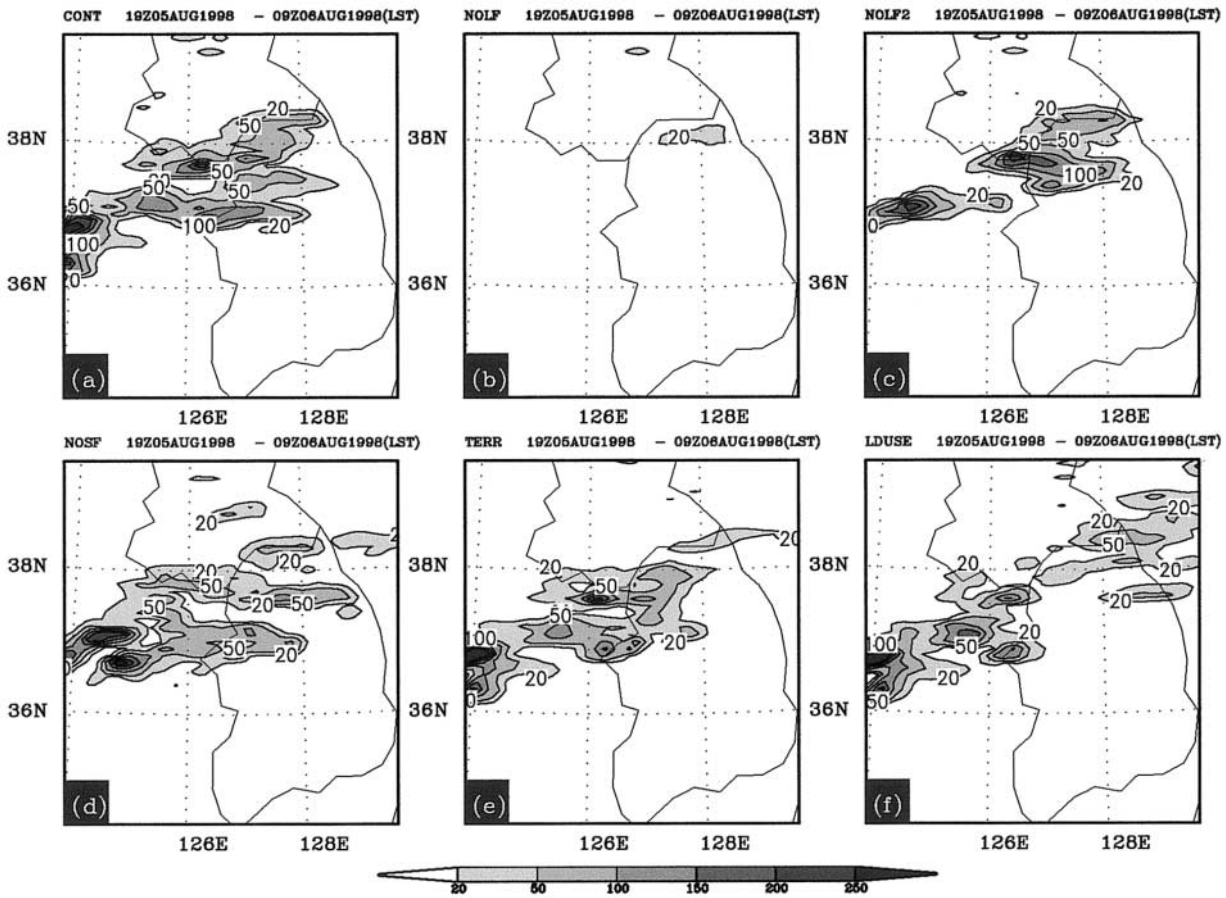

Fig. 17. Simulated rainfall amount for the period 1900 LST 5 (1000 UTC 5)–0900 LST 6 (0000 UTC 6) August 1998 from the control and sensitivity experiments: (a) CONT, (b) NOLF, (c) NOLF2, (d) NOSF, (e) TERR and (f) LDUSE. Contour values are 20, 50, 100, 150, 200, 250 mm, and the areas with the amount above 20 mm are shaded.

level convergence line. This convergence is an important factor for the evolution of the convection band. Neglect of latent heat flux from the surface leads to a weak or negligible development of convection and, consequently, a low-level convergence line does not develop in the NOLF experiment (not shown).

However, when the latent heat flux is considered during the initial 9 hours only (NOLF2), the rainfall pattern is comparable to that in CONT, except for the smaller rainfall area (Fig. 17c). The time and location of convergence-line formation are similar to those in CONT (not shown). The differences between the results of NOLF and NOLF2 appear to exhibit that H_L during the daytime is important for the development of convective systems. Results of NOLF2 also indicate that the surface latent heat flux may not be crucial for the maintenance of convection band and heavy rain development. Since the surface fluxes over the land reach a maximum around noon and become relatively small at night, it is easy to understand the importance of daytime surface fluxes.

Neglect of sensible heat flux does not make a drastic change in the simulated rainfall distribution except that the precipitation in NOSF is not as intense as that in CONT (Fig. 17d). When both the latent and sensible heat fluxes are assumed to be 0 (NOFL), the simulated results are quite similar to those of NOLF (not shown). In the meantime, cutting the surface moisture flux into the air in NOEV does not significantly change the results of CONT, although it has caused the convection to be rela-

tively weaker than that in CONT (not shown). This indicates that the moisture supply into the low-level air from the surface is not an essential element for the formation of convection band.

The assumption of the flat terrain over the Korean peninsula (TERR) also does not make a drastic change to precipitation, except that both the amount and area of precipitation are somewhat less than those of CONT (Fig. 17e). It appears that the Korean topography just affects the intensity of deep convection and is not an essential factor for the formation of convection band in this case. Therefore, the influences of topography are not under the scope of the present study.

When the Korean peninsula is replaced by the sea surface (LDUSE), the rainfall amount decreases in the western part of the peninsula, but increases in the eastern part of the domain when compared to that of CONT. An adequate explanation is not available at present for these changes in rainfall amount. The effect of land use on the convection is an interesting subject for a future study. In the following part, only the impact of land use on surface fluxes will be investigated.

5.2 *The influence of surface fluxes on the lower atmosphere*

Surface latent heat flux may affect the development of convection through its influences on the lower atmosphere: modulation of surface sensible heat flux and direct moisture supply to the low-level air. Hence, further investigations are carried out to understand how the surface fluxes influence the low-level environment in relation to the development of convection.

Figure 18 shows the vertical distributions of specific humidity, and pseudo-equivalent potential temperature (θ_{se}), averaged over the domain enclosed by 125–129°E and 37–38°N (indicated as a box in Fig. 8) for 1500, 1900 and 2100 LST 5 August for the control and sensitivity experiments. These domain-averaged profiles may represent the evolution of environmental condition over the area of convection band formation. Since the simulated convective cells over the sea develop after 1900 LST, the profiles for 1500 and 1900 LST may show the pre-formation condition. At 1500 LST, the low-level specific humidity for NOLF is significantly smaller than those for the other experiments including NOFL, in which both H_L and H_S are neglected. However, the humidity at 850 hPa for NOLF is higher than those for the other experiments. The higher humidity at 850 hPa seems to be caused by the stronger transport of moisture from the lower levels in NOLF. This, and the difference of low-level humidity between NOLF and NOFL, indicate that the decrease of low-level moisture in NOLF is mainly due to vertical diffusion enhanced by the neglect of H_L. Cutting the direct moisture supply into the air in NOEV does not contribute very much to this decrease of low-level moisture, according to the comparison of moisture profiles from NOEV and CONT. Later, discussions will be made to explain further the decrease of low-level moisture, and the role of surface latent heat flux in the band formation.

The specific humidity at the lowest level shows an increase with time except for NOSF, in which it keeps nearly the same value as that for 1500 LST (Fig. 18b). Some changes can be noticed at 2100 LST at the lowest level (Fig. 18c). NOLF and NOFL show similar values of specific humidity, mainly due to the increase in NOLF and small change in NOFL after 19 LST. The other three experiments show noticeably larger humidity than NOLF and NOFL. Significant increases of humidity are found in CONT and LDUSE, especially for CONT. The moisture advection from the sea seems responsible for the increase of humidity in NOLF. However, both the moisture advection and surface latent heat flux appear to be the major reason for the humidity increases in CONT and LDUSE. This indicates that the moisture supply from the surface can also contribute to the increase of convective instability during the late afternoon hours.

As a result of the smaller specific humidity for NOLF, the average θ_{se} at the lowest level is 10∼12 K lower for NOLF (Figs. 18d, e, and f). Consequently, the sounding for NOLF is significantly more stable. Malkus and Riehl (1960) have shown that surface fluxes in the inner core of hurricanes are capable of increasing θ_e by more than 10 K, which contributes significantly to the intensification of a hurricane. Wang et al. (1996) have indicated that H_L, or evaporation from the ocean, is the most influential factor among the three fluxes (latent

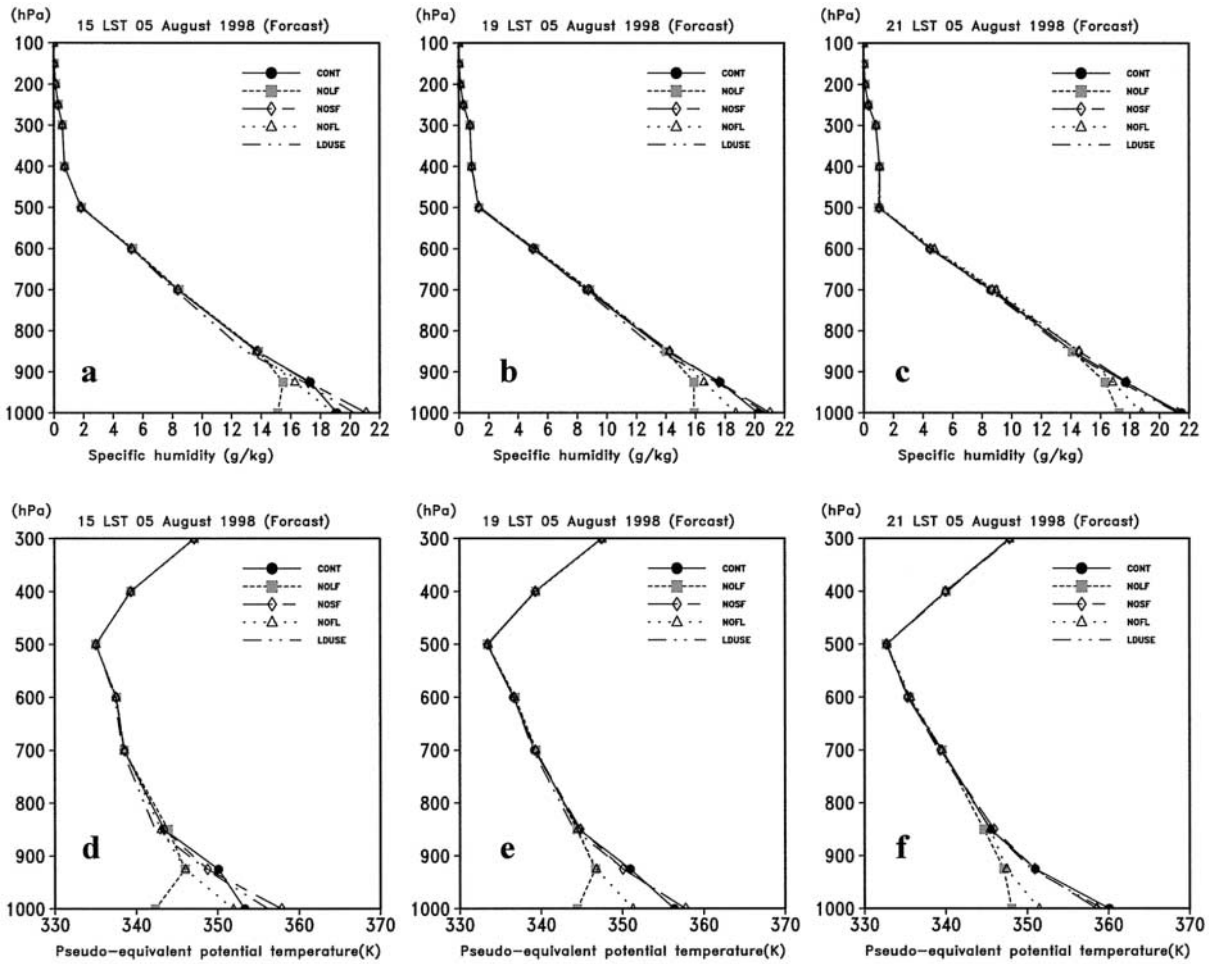

Fig. 18. Vertical distribution of specific humidity for a) 15 LST, b) 19 LST, c) 21 LST 5 August and pseudo-equivalent potential temperature for d) 15 LST, e) 19 LST, f) 21 LST 5 August averaged over the domain enclosed by 37–38°N, 125–129°E (area shown in Fig. 8) in the control (CONT) and sensitivity experiments (NOLF, NOSF, NOFL and LDUSE).

heat, sensible heat, and momentum) for the development of a squall line system. For the present case, surface latent heat flux over the land seems to play a crucial role in the development of convection band by maintaining the convective instability of the lower troposphere.

5.3 *The variation of surface fluxes in sensitivity experiments*

Figure 19 shows the time series of H_L, H_S and the planetary boundary layer (PBL) height averaged over the domain enclosed by 125–129°E, and 37–38°N for control and sensitivity experiments. The magnitude of H_L is 40∼110 Wm^{-2} larger than that of H_S throughout the simulation in the CONT experiment (Figs. 19a and b). On the other hand, the magnitude of H_S is less than 40 Wm^{-2} all day over the sea, while H_L is in the range of 150–250 Wm^{-2} (LDUSE case). Therefore, both H_L and H_S are important over the land, while H_L dominates H_S over the sea.

Although it can be easily understood that H_L is the most influential factor over the sea, it is not very clear why H_L can also be a very important factor over the land. In this study, the value of H_S increases by 20∼110 Wm^{-2} in the daytime when H_L is ignored (NOLF), but is almost the same as that in CONT after 20 LST. On the other hand, the latent heat flux from NOSF is comparable to that of CONT, even though the sensible heat flux is set to 0.

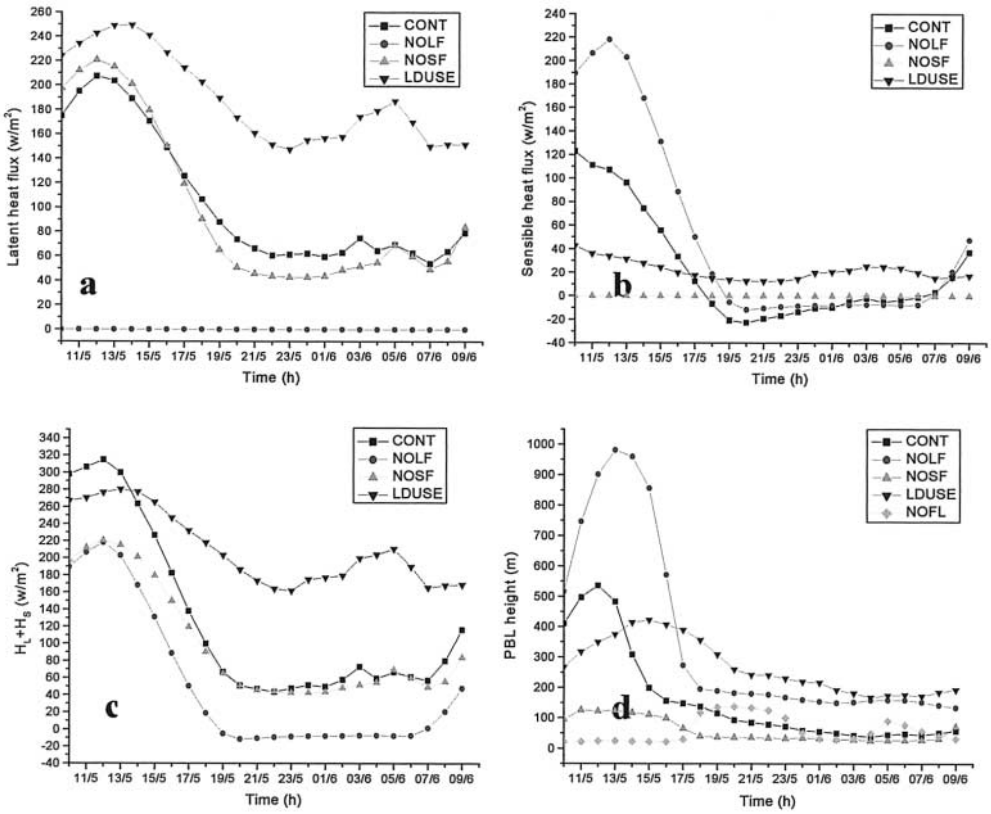

Fig. 19. Temporal variation of a) latent heat flux, b) sensible heat flux, c) total amount of latent and sensible heat fluxes, and d) height of planetary boundary layer averaged over the domain enclosed by 37–38°N, 125–129°E.

Segal et al. (1995) has indicated that the increased H_S usually results in a reduction of specific humidity, and deep convection potential of the convective boundary layer (CBL), due to entrainment of the relatively dry air from above the CBL, and dilution of moisture due to the deepening of CBL. Similar findings are obtained in the present results. Fig. 19d shows the time series of averaged PBL height for the control and sensitivity experiments. Here, the PBL height is defined as the top of the mixed layer. PBL height is 100–700 m higher during the daytime in NOLF than that for CONT, mainly due to the larger H_S for NOLF. This increased PBL height results in a decrease of specific humidity at lower levels, and consequently a smaller potential for moist convection in NOLF. Hence, too large H_S caused by ignoring H_L, seems to be very important in making the lower tropospheric environment unfavorable for the convection development in NOLF.

On the other hand, a small H_S during the daytime may also decrease the intensity of deep convection over the land at the nighttime as noted in the decreased amount of rainfall over the land without sensible heat flux in NOSF.

The results indicate that the surface latent heat flux is an essential element for the formation of convection band. Its major role is found to be in its contribution to the maintenance of the favorable environment for convection formation. The surface latent heat flux plays the key role in maintaining sufficient conditional instability, especially during the daytime, by modulating the surface sensible heat flux over the land area. Modulation of sensible heat flux limits PBL depth and dilution of low-level moisture to a certain level maintaining convection potential over the land. In the present case, the moisture supply from the land surface does not affect the formation of convection band as much as the modulation of surface sensible heat flux by the surface latent heat flux. But it

can contribute to the increase of convective instability of low-level air during the late afternoon hours.

6. Summary and conclusions

An investigation has been carried out to explain the formation and development of the intense long-lived quasi-stationary convection band that occurred on 5–6 August 1998 over the middle part of the Korean peninsula. First, the weather conditions have been analyzed using observational data. Second, numerical simulations have been carried out using the PSU/NCAR mesoscale model (MM5) with a nested fine-mesh grid size of 5 km.

Radar observation indicates that the convection band is 20–30 km wide, and about 300 km long at its mature stage. This convection band persisted for more than 10 hours without moving to any great degree, and consisted of several long-lived precipitation cells along the band. It has been found that the precipitation cells develop on the west coast and move northeastward along the band. The synoptic analysis indicates that the convection band has occurred between a mid latitude cyclone (to the north of the Korean peninsula) and the western Pacific subtropical high (WPSH). A converging flow pattern is found at lower levels over the middle of the Korean peninsula between the westerly to the north, and the southwesterly to the south of the band. The low level southwesterly transports moist air to the area of convection. These provide a favorable environment for the formation and maintenance of the long-lived quasi-stationary convection band.

The simulated convection band appears to form and evolve in a consistent manner with the observation. Its location and extent also agree with the observation. On the other hand, it shows several differences from the observation in the onset time, lifetime and rainfall intensity, etc. The simulated convection band in the early and mature stage consists of long-lived cells that propagate northeastward along the band.

The formation of the simulated convection band proceeds in the following manner. First, new convection cells continuously form at the western coast and move northeastward forming a line of long-living convection cells. Second, a line of low-level convergence forms in the upwind side of the convection initiation point, and then, convective cells develop and move along this line. Some cells develop into deep convection as they move, and last several hours. These processes result in a long convection band.

The convection band develops in the area of large-scale converging airflow over the middle of the Korean peninsula. This favorable large-scale condition and its interaction with convection seem to be important for the development of the present convection band. The convection cells are found to move along the prevailing wind direction at low levels below 800 hPa in this region and enhance the flow convergence contributing to the development of a sharp convergence line, which then supports the development and maintenance of the propagating convection cells.

The simulated convection cells at mature stage have a structure that can maintain convection: 1) warm and moist air is continuously supplied by the low-level inflow ahead of the band; 2) updraft tilts northward at levels below 2 km, but stands upright above 2 km; 3) a cooler downdraft develops in the precipitation area behind the inflow region; and, enhances the low-level convergence between the downdraft and the inflow air.

Several sensitivity experiments have been performed to isolate the impacts of different surface forcings on the initiation and development of the convection band. The convection band does not form without surface latent heat flux. Surface latent heat flux is found to play a crucial role in establishing a convectively unstable environment by modulating the surface sensible heat flux over the land. It is also found that orographic effect is not an essential factor for the formation of the present convection band.

The present study has some limitations in verification of numerical results. The detailed structure of the convection band, such as the updraft and downdraft, cannot be verified by observation because high-resolution observation is not available. In the meantime, some questions remain to be studied further. They include; 1) the precise triggering mechanism of convection on the west coast, and 2) the mechanism of the initial formation of the convergence line over the sea.

Acknowledgments

This study has been supported by the Ministry of Science and Technology through the National Research Laboratory Program and by the Ministry of Education through the BK21 Program. The authors are especially grateful to the anonymous reviewers for their valuable comments, which have contributed to the significant improvement of this paper.

References

Akiyama, T., 1979: Thermal stratification in Baiu frontal medium-scale disturbances with heavy rainfalls. *J. Meteor. Soc. Japan*, **57**, 587–598.

Blackadar, A.K., 1979: High resolution models of the planetary boundary layer. *Advances in Environmental Science and Engineering*, J.R. Pfaflin and E.N. Zeigler, Eds., Gordon and Breach. 50–85.

Chen, G.T.J., 1983: Observational aspects of the Mei-yu phenomenon in subtropical China. *J. Meteor. Soc. Japan*, **61**, 306–312.

Chen, G.T.-J. and C.-C. Yu, 1988: Study of low-level jet and extremely heavy rainfall over northern Taiwan in the Mei-yu Season. *Mon. Wea. Rev.*, **116**, 884–891.

Chen, Q., 1982: The instability of the gravity-inertia wave and its relationship to low-level jet and heavy rainfall. *J. Meteor. Soc. Japan*, **60**, 1041–1057.

Dudhia, J., 1996: A multi-layer soil temperature model for MM5. *Preprints, The sixth PSU/NCAR mesoscale model user's workshop*, 22–24 July 1996, Boulder, Colorado, 49–50.

Grell, G.A., Y.-H. Kuo and R.J. Pasch, 1991: Semi-prognostic tests of cumulus parameterization schemes in the middle latitudes. *Mon. Wea. Rev.*, **119**, 5–31.

Hwang, S.-O. and D.-K. Lee, 1993: A study on the relationship between heavy rainfalls and associated low-level jets in the Korean peninsula. *J. Korean Meteor. Soc.*, **29**, 133–146 (in Korean).

Hoskins, B.J., I. Draghici and H.C., Davies, 1978: A new look at the ω-equation. *Quart. J. Roy. Meteor. Soc.*, **104**, 31–38.

Kim, S.S., C.H. Chung, S.U. Park and B.S. Lee, 1983: The characteristic structural difference of the rainy front (Changma front) between the wet and dry season. *J. Korean Meteor. Soc.*, **19**, 12–32 (in Korean).

KMA (Korea Meteorological Administration), 2001: Climatological standard normals of Korea (1971–2000). To be published.

Laing, A.G. and J.M. Fritsch, 1997: The global population of mesoscale convective complexes. *Quart. J. Roy. Meteor. Soc.*, **123**, 389–405.

Lee, T.-Y., Y.-Y. Park and Y.-H. Kim, 1998: A numerical modeling study of heavy rainfall development over the Changma front. *Proceedings of the International Conference on Monsoon and Hydrologic Cycle, April 22–25, 1998*, Kyongju, Korea, 72–75.

Li, J., Y.-L. Chen and W.-C. Lee, 1997: Analysis of a heavy rainfall event during TAMEX. *Mon. Wea. Rev.*, **125**, 1060–1082.

Maddox, R.A., 1983: Large-scale meteorological conditions associated with midlatitude, mesoscale convective complexes. *Mon. Wea. Rev.*, **111**, 1475–1493.

Malkus, J.S. and H. Riehl, 1960: On the dynamics and energy transformations in steady-state hurricanes. *Tellus*, **12**, 1–20.

Matsumoto, S., 1973: Lower tropospheric wind speed and precipitation activity. *J. Meteor. Soc. Japan*, **51**, 101–107.

Ninomiya, K. and T. Akiyama, 1974: Band structure of mesoscale clusters associated with low level jet stream. *J. Meteor. Soc. Japan*, **52**, 300–313.

———, ——— and M. Ikawa, 1988: Evolution and fine structure of a long-lived meso-α-scale convective system in Baiu frontal zone. Part I: Evolution and meso-β-scale characteristics. *J. Meteor. Soc. Japan*, **66**, 331–350.

——— and T. Murakami, 1987: The early summer rainy season (Baiu) over Japan. *Monsoon Meteorology*, C.P. Chang and T.N. Krishnamurthi, Eds., Oxford University Press, 93–121.

——— and K. Yamazaki, 1979: Heavy rainfall associated with frontal depression in Asian subtropical humid region. Part II: Mesoscale features of precipitation, radar echoes and stratification. *J. Meteor. Soc. Japan*, **57**, 399–413.

Ogura, Y., T. Asai and K. Dohi, 1985: A case study of a heavy precipitation event along the Baiu front in northern Kyushu, 23 July 1982: Nagasaki heavy rainfall. *J. Meteor. Soc. Japan*, **63**, 883–900.

Park, S.-U., I.-H. Yoon and S.-K. Chung, 1986: Heat and moisture sources associated with Changma front during the summer of 1978. *J. Korean Meteor. Soc.*, **22**, 1–27 (in Korean).

Reisner, J., R.T. Bruintjes and R.J. Rasmussen, 1998: Explicit forecasting of supercooled water in winter stroms using the MM5 mesoscale model. *Quart. J. Roy. Meteor. Soc.*, **124B**, 1071–1107.

Rotunno, R. and K.A. Emannuel, 1987: An air-sea interaction theory for tropical cyclones. Part II: Evolutionary study using a nonhydrostatic

axisymmetric numerical model. *J. Atmos. Sci*., **44**, 542–561.

Segal, M., R.W. Arritt, C. Clark, R. Rabin and J. Brown, 1995: Scaling evaluation of the effect of surface characteristics on potential for deep convection over uniform terrain. *Mon. Wea. Rev*., **123**, 383–400.

Shapiro, M.A. and P.J. Kennedy, 1981: Research aircraft measurements of jet stream geostrophic and ageostrophic winds. *J. Atmos. Sci*., **38**, 2642–2652.

Tao, S. and L. Chen, 1987: A review of recent research on the East Asian summer Monsoon in China. *Monsoon Meteorology*, C.P. Chang and T.N. Krishnamurthi, Eds., Oxford University Press, 60–92.

Tao, W.-K. and S.-T. Soong, 1991: Numerical simulation of a subtropical squall line over Taiwan Strait. *Mon. Wea. Rev*., **119**, 2699–2723.

Teng, J.-H., C.-S. Chen, T.-C.C. Wang and Y.-L. Chen, 2000: Orographic effects on a squall line system over Taiwan. *Mon. Wea. Rev*., **128**, 1123–1138.

Wang, Y., W.-K. Tao and J. Simpson, 1996: The impact of ocean surface fluxes on a TOGA COARE convective system. *Mon. Wea. Rev.*, **124**, 2753–2763.

Yoshizaki, M., T. Kato, Y. Tanaka, H. Takayama, Y. Shoji, H. Seko, K. Manabe and Members of X-BAIU-98 Observation, 2000: Analytical and numerical study of the 26 June 1998 orographic rainband observed in western Kyushu, Japan. *J. Meteor. Soc. Japan*, **78**, 835–856.

Yoshizumi, S., 1975: Development of an instability line under a cut-off low, *Pap. Meteor. Geophy*., **26**, 167–180.

Yu, C.-K., B.J.-D. Jou and B.F. Smull, 1999: Formative stage of a long-lived mesoscale vortex observed by airborne Doppler radar. *Mon. Wea. Rev*., **127**, 838–857.

Zhang, D.L. and R.A. Anthes, 1982: A high-resolution model of the planetary boundary layer-Sensitivity tests and comparisons with SESAME-79 data. *J. Appl. Meteor*., **21**, 1594–1609.